Construction and Building Materials 462 (2025) 139981

Contents lists available at ScienceDirect

Construction and Building Materials

journal homepage: www.elsevier.com/locate/conbuildmat

Engineering aluminosilicates with high surface area extracted from waste concrete to form a viable supplementary cementitious material

Tiejun Ding *, Suyang Zhang, Marcus Yio, Hong Wong, Christopher Cheeseman

Centre for Infrastructure Materials, Department of Civil and Environmental Engineering, Imperial College London, London SW7 2AZ, United Kingdom

ARTICLE INFO

Keywords:
Low-carbon cement
Heat treatment
Workability
Pozzolanic
Circular economy

ABSTRACT

Aluminosilicate residues can be produced by acid leaching waste concrete. These are pozzolanic and have the potential to be used as a supplementary cementitious material (SCM). However, the workability of cement mixes is seriously compromised when aluminosilicate particles are used, due to their high surface area and excessive water absorption. This negatively influences the compaction and performance of mixes. In this work, aluminosilicates extracted from waste concrete have been heat-treated, and the effects of temperature on their specific surface area, pozzolanic reactivity, and consequently the workability and strength of mortars are reported. Thermal treatment at 900℃ for 1 hour reduces the specific surface area of aluminosilicate particles to values comparable to commercial SCMs such as coal fly ash (FA) and ground granulated blast furnace slag (GGBFS), while retaining significant pozzolanic activity. Mortars containing CEM I replaced by 20 wt% of optimally heat-treated aluminosilicate residue at a 0.56 w/b ratio show improved flow properties compared to untreated residues, and similar compressive strength to mortars containing the same amount of silica fume (SF) or GGBFS. The research shows that aluminosilicates extracted from cement paste can be heat treated to form a viable SCM, and this contributes to the future development of circular concrete.

1. Introduction

More than 2.5 billion tonnes of construction and demolition waste are produced globally each year, of which between 60 and 80 wt% is waste concrete [1,2]. Concrete recycling normally involves crushing and size sorting to produce relatively low-grade recycled concrete aggregate. This contains cement mortar adhered to primary aggregate, which increases the porosity and water absorption of the recycled aggregate, limiting use in new concrete [3,4]. In addition, current concrete recycling generates a fine powder waste that mainly consists of hydrated cement paste, sand, and unreacted cement particles. This is usually landfilled and represents a waste of a potentially valuable resource [5]. Upcycling waste concrete powder has become increasingly important and is an active research area [6]. Accelerated carbonation can effectively transform waste concrete into value-added products and sequester CO_2.

Direct carbonation involves bubbling CO_2 into a mixture of waste concrete powder and water. This produces $CaCO_3$ and amorphous aluminosilicate gel [7–10]. The morphology of the precipitated $CaCO_3$ is controlled by varying the temperature and incorporating chemical additives such as Mg^{2+} to improve the reactivity of the carbonated waste concrete powder [7,11]. The carbonated waste concrete powder is characterised by high pozzolanic reactivity and a high specific surface area of 41.9 m^2/g [12]. Direct carbonation processes are simple and relatively low-cost, but the carbon capture potential depends on the extent of carbonation and the amount of material that can be carbonated in the waste concrete [13].

Indirect carbonation involves dissolving waste concrete powder in an acid or alkali solution and sequestering CO_2 by reaction with the resulting solution. This produces an aluminosilicate gel from C-S-H and C-A-S-H phases, and precipitates $CaCO_3$ [14–17]. The aluminosilicate gel consists of agglomerated nanosized particles and has pozzolanic reactivity [17,18]. Indirect carbonation is more complex than direct carbonation, but has the potential to achieve complete carbonation and sequester more CO_2 because Ca^{2+} ions are released from the dissolution of C-S-H and C-A-S-H. Furthermore, the aluminosilicate gel and pure $CaCO_3$ formed can be used in higher-value applications.

Developing novel supplementary cementitious materials (SCM) is important, because conventional SCMs such as coal fly ash (FA), ground granulated blast furnace slag (GGBFS) and silica fume (SF), have limited

* Corresponding author.
E-mail address: tiejun.ding18@imperial.ac.uk (T. Ding).

https://doi.org/10.1016/j.conbuildmat.2025.139981
Received 12 October 2024; Received in revised form 12 December 2024; Accepted 11 January 2025
Available online 16 January 2025

global availability [19]. In 2022, 0.53 billion tonnes of GGBFS were produced, accounting for only 13 % of global cement production [20]. Similarly, the global supply of coal fly ash (FA) is between 0.6 and 0.9 billion tonnes per year, and that of silica fume (SF) is only between 1 and 2.5 million tonnes per year. Therefore, these conventional SCMs are valuable resources with limited potential for decarbonising the cement industry at high substitution levels.

Given the enormous amounts of waste concrete, extracting viable aluminosilicate SCMs with carbonation to form $CaCO_3$ to make low-carbon construction materials, is an interesting option. The high specific surface area of the aluminosilicate gel has been found to improve the early stage pozzolanic reactivity [8,21]. However, high specific surface area is associated with high water absorption, reducing the workability of concrete and making use as a viable SCM problematic. Waste concrete powder carbonated by a wet carbonation process at 25℃ using pure CO_2 had a specific surface area of 56.54 m^2/g. 20 % replacement of CEM I by the carbonated waste concrete powder caused ~50 % decrease in the paste flow without vibration [21].

The specific surface area of carbonated concrete fines can be reduced using a modified direct carbonation process. A semi-dry direct carbonation process for waste concrete powder has been developed [7]. In this, pure CO_2 in saturated water vapour at elevated temperatures (45 – 55℃) was used. Compared to waste concrete powder carbonated in solution, the BET surface area of semi-dry carbonated waste concrete powder was reduced by 36 %. However, the resulting surface area remained high (~34 m^2/g). In another study, monoethanolamine (MEA) was added during the direct carbonation of WCP to increase the repulsion of carbonated WCP particles and unlock the trapped water. Cement paste containing 30 % of WCP carbonated in 45 % MEA solution resulted in the same flowability as the reference consisting of 100 % CEM I [22]. However, this method resulted in low early-age strength and increased cost. To our knowledge, there has not been any reported research focusing on improving the workability of the aluminosilicate SCM extracted by indirect carbonation of waste concrete powder.

In our previous research, acetic acid has been used to leach waste concrete fine aggregates and cement paste powder, generating clean sand, an aluminosilicate residue (SR), and a calcium-rich solution that can be converted into calcium carbonate via reaction with CO_2 [18,23]. The SR mainly consists of amorphous aluminosilicate gel with crystalline impurities, such as quartz. The Frattini test showed that the SR had comparable pozzolanic reactivity to fly ash, indicating its potential as an SCM. However, the SR significantly reduced the workability of cement mortar. A superplasticiser dosage of 5 % was needed to achieve good workability, leading to additional costs [23]. Therefore, there is a need to process the SR to improve workability.

Sintering converts compacted ceramic powder samples into more dense structures, typically using temperatures above 1000℃. It has been used to densify silica and alumina-rich industrial wastes, such as fly ash to produce glass ceramics and lightweight aggregates. During sintering, particles fuse to form bonding between adjacent particles and close the pores, reducing the specific surface area [24–26]. Inspired by this phenomenon, this research uses heat treatment to reduce the specific surface area of SR, so as to improve the workability of SR-blended cement mortars. The effect of heat treatment temperature on the particle size distribution, specific surface area and pozzolanic reactivity of SR are reported. The impact of the treated SR on the hydration kinetics, workability and compressive strength of cement mortars are also reported. The temperature-induced microstructural changes are characterised, and the potential use of heat-treated SR extracted from waste concrete is discussed.

2. Experimental

2.1. Materials

Simulated waste concrete powder was produced from hydrated cement paste (HCP), by mixing tap water with CEM I 52.5 N (Breedon, UK) at a water/cement ratio of 0.4. The mix was cured for 24 hours in a sealed plastic bag. The hardened mix was then immersed in a saturated lime solution, where it was hydrated at 20℃ for 90 days. The HCP was then dried at 40℃ to a constant mass and ground using a mortar and pestle to pass through a 300 μm sieve. The chemical compositions of CEM I and HCP are shown in Table 1. Glacial acetic acid (VWR, UK) was diluted with deionised water to form a 1.6 mol/L acetic acid solution for leaching of cement paste. Thames River siliceous sand (< 4 mm), CEM I 52.5 N (Breedon, UK), commercially available silica fume (SF, Elkem Norway), ground granulated blast-furnace slag (GGBFS, Heidelberg Materials Germany) and class-F fly ash (FA, Heidelberg Materials Germany) were used to prepare mortar samples (Section 2.5).

2.2. Production of SR

The production of SR follows the method described in our previous paper [23]. Briefly, 180 g of HCP is reacted with 2 L of 1.6 mol/L acetic acid for 1 hour at 60℃. The resulting slurry from acid leaching was centrifuged at 3000 rpm for 3 minutes, and vacuum filtered to collect the SR. After thoroughly rinsing with deionised water, the SR was dried at 60℃ to a constant mass, and then ground into a powder (< 300 μm) using a mortar and pestle.

10 g of powdered SR samples were heated in a porcelain crucible to 840, 870, 900, 950 and 1000℃ for 1 hour in a furnace (Carbolite Gero HTF 17/5). These temperatures were selected based on the TGA-DSC results, as discussed later (Section 3.1). The heat-treated SR samples were cooled to room temperature in the furnace, and were labelled SR840, SR870, SR900, SR950 and SR1000, respectively. After heating, SR840, SR870 and SR900 remained as powder, while SR950 and SR1000 formed hard particles, and they were ground to less than 300 μm using a mortar and pestle before subsequent experiments.

Apart from the abovementioned samples, SR samples heated at 250, 400, 600, 700 and 800℃ were also prepared for specific surface area and R^3 cumulative heat measurements to study the effect of temperature on the surface area and pozzolanic reactivity of the SR.

2.3. Characterisation methods

Thermogravimetry analysis (TGA-DSC, Netzsch STA 449 F5) was conducted to determine the sintering temperature range and loss-on-ignition (LOI) using ~20 mg of powdered samples, heated under N_2 flow from 30 to 1050℃, at a heating rate of 10 ℃/min and an N_2 flow rate of 50 mL/min. The LOI was calculated from the mass difference of the samples between 30℃ and 1050℃. The chemical composition of test materials was determined using X-ray fluorescence (XRF, Malvern Panalytical Zetium). The crystalline phases present were determined using X-ray diffraction (XRD, Malvern Panalytical Empyrean) with Cu Kα radiation. The scan was performed at a speed of 0.044 degrees per minute over a 2θ range of 5–70°. To determine the phase composition, Rietveld refinement was performed, using 20 wt% corundum (Al_2O_3) as an internal standard, with analysis using HighScore Plus software. The amorphous content was calculated from Eq. (1).

$$C_{am}\% = \frac{5}{4}\left(100 - 20 \times \frac{100}{C_{co}\%}\right) \quad (1)$$

where C_{am}% is the amorphous content of the sample, and C_{co}% is the corundum content determined by Rietveld refinement.

Fourier transform infrared adsorption spectroscopy (FTIR, Thermofisher Nicolet iS50) was performed on powder samples in the attenuated total reflection mode to analyse the chemical bonding in SR. The specific surface area of untreated and heat-treated SR was determined as an average of three measurements using N_2 adsorption (Micromeritics 3Flex 3500). The samples were degassed at 40℃ under vacuum for 24 hours and the specific surface area was calculated from the adsorbed

Table 1
Chemical composition expressed as oxide % and LOI of CEM I and the test materials.

Sample	Percentage (%)							
	SiO_2	Al_2O_3	CaO	Fe_2O_3	MgO	TiO_2	K_2O	SO_3	LOI
CEM I 52.5 N	18.47	5.47	63.62	2.75	0.99	0.28	0.72	3.71	3.24
HCP	13.52	4.10	48.04	2.22	0.85	-	0.34	2.76	27.36
SR untreated	51.50	13.56	5.19	3.71	0.49	0.65	0.46	0.16	23.38
SR840	65.28	17.29	6.98	5.12	0.68	0.81	0.70	0.47	0.31
SR870	66.16	17.43	6.93	5.28	0.64	0.78	0.75	0.40	0.28
SR900	67.05	17.56	6.93	5.08	0.65	0.82	0.71	0.40	0.24
SR950	67.72	17.82	6.53	4.64	0.65	0.84	0.58	0.31	0.15
SR1000	67.84	17.86	6.54	4.67	0.66	0.85	0.58	0.31	0.07
SF	93.27	0.42	0.28	0.21	0.47	-	1.58	0.41	2.32
GGBFS	33.72	11.43	40.63	0.56	5.88	1.31	0.68	1.72	3.05
FA	51.29	25.74	4.79	6.51	1.51	1.45	1.41	0.44	2.27

gas volume in accordance with the Brunauer-Emmett-Teller (BET) theory. The particle size distribution of the untreated and heat-treated SR was measured using laser diffraction (Malvern Mastersizer 3000). Tap water was used as the dispersant because the material's stability in water ensured reliable and reproducible measurements. The d_{10}, d_{50} and d_{90} values were calculated as the average of five measurements. The particle morphology of SR was observed using scanning electron microscopy (SEM, Zeiss Sigma 500VP FESEM) on carbon-coated samples in the secondary electron (SE) mode. The microstructure of 28-day mortar samples was examined using surface-polished sample blocks in the back scattered electron (BSE) mode. The C-S-H composition was determined by energy dispersive spectrometry (EDS) under an accelerating voltage of 15 kV.

2.4. Pozzolanic reactivity (R^3) and heat of hydration

The R^3 test was used to assess the pozzolanic reactivity of the SR samples. Test samples containing 10 g of the SR, 30 g $Ca(OH)_2$, 5 g $CaCO_3$ and 54 g of the solution containing 20 g/L K_2SO_4, and 4 g/L KOH were prepared [27]. Specifically, 15 g of the sample was tested using isothermal conduction calorimetry (TAM Air) at 40℃ for 7 days, with 9.4 g of deionised water used as a reference for heat change. The 7-day cumulative heat of the test samples was normalised against the mass of SR and plotted against the heat treatment temperature.

Ten cement paste samples, consisting of a 100 % CEM I reference mix, three blended mixes with 20 % CEM I replaced by GGBFS, FA and SF and six blended mixes with 20 % CEM I replaced by untreated SR, SR840, SR870, SR900, SR950 and SR1000 were prepared, with a constant water-to-binder (w/b) mass ratio of 0.4. At this w/b ratio, the mix containing untreated SR is dry and stiff. Therefore, superplasticiser (MasterGlenium 315 C) was added at 5 % wt. of binder to achieve a workable paste and remove entrapped air voids that would otherwise influence measurements. The heat of hydration of paste samples was determined at 20°C for 7 days using isothermal conduction calorimetry (TAM Air) in accordance with British standard [28]. The heat flow and cumulative heat were normalised using the mass of Portland cement in the paste.

2.5. Mortar production, flow properties and strength testing

Mortar samples were prepared using 100 % CEM I (reference) and binders containing 80 % CEM I and 20 % untreated and heat-treated SR. These were compared to mortars containing the same CEM I replacement using FA, SF or GGBFS. CEM I replacement of 20 % is feasible, as shown by the results of previous work [23]. Siliceous sand (< 4 mm) was used as fine aggregate, and the sand-to-binder mass ratio was 3.0. The water-to-binder ratio was set to 0.56 to achieve a workable reference without using superplasticizer. The workability of fresh mortar was assessed using a flow table. Cube samples were cast into 20 × 20 × 20 mm steel moulds and vibrated for 2 minutes. For mortars containing SF or untreated SR, extended vibration of 4 minutes was applied to compensate for the low workability. Test cubes were demoulded after 24 hours and cured in a saturated lime solution at 20 ± 1 ℃ for 3, 7, 28 and 60 days. The compressive strength of mortar cubes was determined using six replicates at each curing age on a universal testing machine (Instron 5980 Universal Testing System).

3. Results

3.1. Physical properties, chemical compositions and pozzolanic reactivity of SR

TGA-DSC data of the untreated SR is shown in Fig. 1. The major mass loss occurs before 200℃. The DSC data shows that an endothermic peak exists at 130℃, which is due to heat absorption from the removal of physically adsorbed water. This agrees with previous research on amorphous silica gel which showed that multi-layer adsorbed water is eliminated to form a monolayer that is then completely removed when the temperature reaches ~200℃ [29]. Above 200℃, silanol condensation occurs when the vicinal silanol, geminal silanol and isolated silanol are condensed and evaporated with increasing temperature [29]. These are not directly observed from the DSC data, because it is masked by other exothermic processes such as the combustion of the adsorbed acetate and densification of the SR, as shown in the exothermic hump and continuous mass loss between 200 and 800℃ [30,31]. A broad exothermic peak is observed in the DSC curve at 870℃, indicating sintering. This is attributed to the release of surface energy due to a reduction in surface area [32]. Therefore, heat treatment temperatures are selected to span this exothermic peak (800–1000℃), as described in Section 2.2.

Table 1 compares the chemical composition of untreated and heat-treated SR to commercially available SCMs and hydrated cement paste

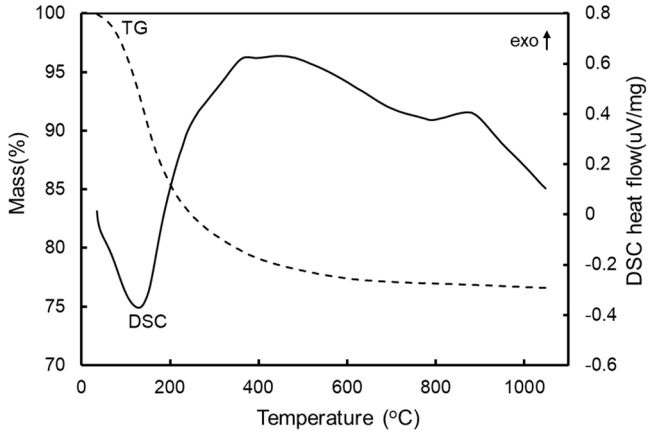

Fig. 1. TGA and DSC curves of the untreated silica-rich residue.

(HCP). Acetic acid treatment of HCP leaches Ca^{2+}, producing a solid residue that contains mainly silica and alumina. Untreated and heat-treated SR have similar chemical composition to class-F fly ash, although with generally higher SiO_2/Al_2O_3 ratio. Heating increases the percentages of the main oxides in the aluminosilicate residue but reduces the loss-on-ignition (LOI) due to removal of physically absorbed water by evaporation, and chemically bound water by silanol condensation.

The XRD data of untreated and heat-treated SR are shown in Fig. 2. Untreated SR is predominantly amorphous with some quartz, which is present in the cement paste and is resistant to acid dissolution. Similar XRD data was obtained for heat-treated SR at temperatures up to 900℃. At higher temperatures a transition from amorphous to crystalline phases occurs. At 950℃, the diffraction peaks of cristobalite (SiO_2) and anorthite ($Ca(Al_2Si_2O_8)$) appear. At 1000℃, the intensity of these peaks increases, and hematite (Fe_2O_3) is detected. QXRD shows that untreated SR, SR840, SR870, SR900, SR950 and SR1000 have amorphous contents of 98.6, 98.8, 98.7, 98.1, 80.7 and 47.6 %, respectively. This indicates that the crystallisation of amorphous aluminosilicate gel in SR commences above 900℃ and this increases with increasing temperature. In comparison, the amorphous contents of SF, GGBFS and FA are 99.1 %, 94.3 % and 65.2 % respectively. All the SR treated below 950℃ have similar amorphous content to SF and GGBFS and are more amorphous than FA.

Fig. 3 shows FTIR results of untreated and heat-treated SR. The absorbance peak at around 800 cm^{-1} is associated with the symmetric stretching of Si-O-Si [33]. The intense peak around 1000 cm^{-1} denotes the asymmetric stretching vibration of Si-O-Si, and this slightly shifts to the right as the temperature increases because of changes in the silica structure. The Si-OH silanol bond is characterised by a peak at 1640 cm^{-1} [34,35]. The wide hump at ~3400 cm^{-1} is formed from hydrogen bonded silanol structures (Si-O-H) [36]. As the heat treatment temperature increases, the peaks associated with absorbed water and silanol at 3400 and 1640 cm^{-1} disappear, corresponding to the evaporation and the condensation of silanol structures. A peak at 470 cm^{-1} emerges at 950℃ and becomes distinct at 1000℃, which is characteristic of cristobalite [37]. At 1000℃, a new peak appears at 916 cm^{-1}, which is characteristic for anorthite [38], and this is consistent with the XRD results.

SEM images showing morphological changes of heat-treated SR are presented in Fig. 4a-f. Fig. 4a indicates that untreated SR contains agglomerates of loosely packed nanosized primary particles. This results in a rough surface, and the space between the nanosized primary particles forms interconnected porosity accessible to N_2. When heated at 840℃ (Fig. 4b), the rough surface texture remains but the primary particles appear larger compared to untreated SR, with dense surfaces starting to form. The sintering is further promoted at 870℃ (Fig. 4c), where more

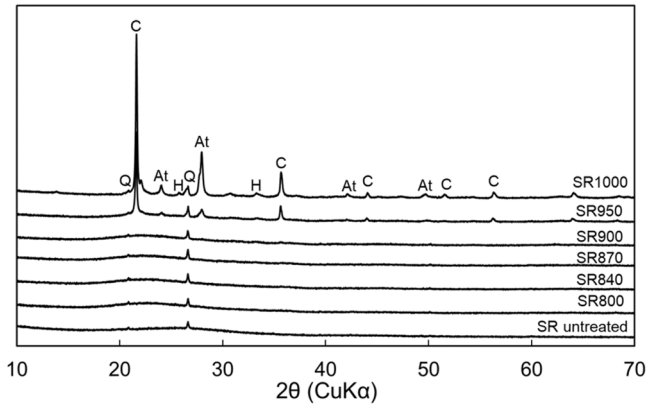

Fig. 2. XRD data of raw and heat-treated silica-rich residue. Q: Quartz; C: Cristobalite; At: Anorthite; H: Hematite.

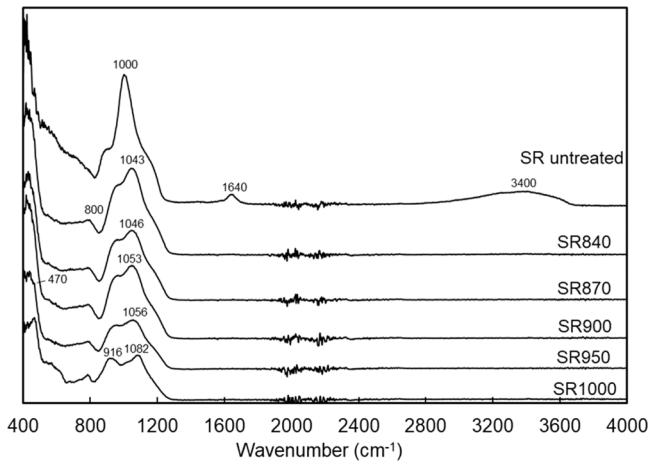

Fig. 3. FTIR-ATR spectra of raw and heat-treated silica-rich residue.

voids between primary particles are closed and smoother surfaces formed. At 900℃ (Fig. 4d), sintered bodies with smoother surfaces have replaced the porous particles. At 950℃ (Fig. 4e), small-sized 0.1 – 0.3 μm crystals are seen on particle surfaces, indicating the sintering process is complete and crystallisation occurs. At 1000℃ (Fig. 4f), the crystals become larger due to increased crystallisation of cristobalite, anorthite and hematite.

The effect of heat treatment temperature on the particle size distribution of SR samples, FA, GGBFS and SF is shown in Table 2. The d_{10} and d_{50} of SR increase with temperature because small particles melt and form larger agglomerates during sintering. The d_{90} of SR slightly decreases from 840 to 900℃, indicating that there is some breakdown of larger particles during sintering. The particle size of SR samples is greater than FA, GGBFS and SF.

The effect of temperature on the pozzolanic reactivity (R^3) and specific surface area of SR is shown in Fig. 5. In Fig. 5a, untreated SR releases 250 J/g during 7 days of pozzolanic reaction. After heat treatment up to 700℃, the amount of heat released at 7 days increased by a factor of 2. This is due to the removal of physically adsorbed and chemically bound water, which increases the concentration of the reactive silica and alumina as shown in Table 1. The specific surface area of untreated SR (154.95 m^2/g) is around 120 times as that of FA (1.26 m^2/g) and GGBFS (1.42 m^2/g) and about 7 times that of SF (22.80 m^2/g). Given that untreated SR has a larger particle size, this indicates that untreated SR is highly porous. The specific surface area of SR is reduced by around 50 % at 700℃. This is caused by silanol condensation which forms 'necks' through Si-O-Si bonding between the nanosized grains and closes the pores as suggested by literature [39].

With increasing temperature from 700℃ to 900℃, the specific surface area greatly decreases. Above 840℃ it falls within the range of FA, GGBFS and SF as shown in Fig. 5b. This is because sintering occurs in this temperature range, which closes voids and produces larger particles with lower surface energy and surface area. On the other hand, this reduces the dissolution rate and provides fewer nucleation sites for the growth of cement hydration products, resulting in reduced pozzolanic reactivity of SR from 467 to 307 J/g.

Above 900℃, the reduction in surface area is much slower and almost plateaus, while the pozzolanic reactivity of SR is drastically reduced. This suggests that the sintering of aluminosilicate gel in the SR is complete at around 900℃, and further reductions in pozzolanic reactivity are caused by crystallisation which shields the amorphous silica [40]. A material is highly pozzolanic, moderately pozzolanic and inert when the 7-day R^3 cumulative heat release is > 200, 100 – 200 and < 100 J/g, respectively [41]. SR870 and SR900 have a surface area of 6.5 and 2.1 m^2/g, and 7-day heat release of 403 and 307 J/g, respectively. This indicates that a heat treatment temperature between 870

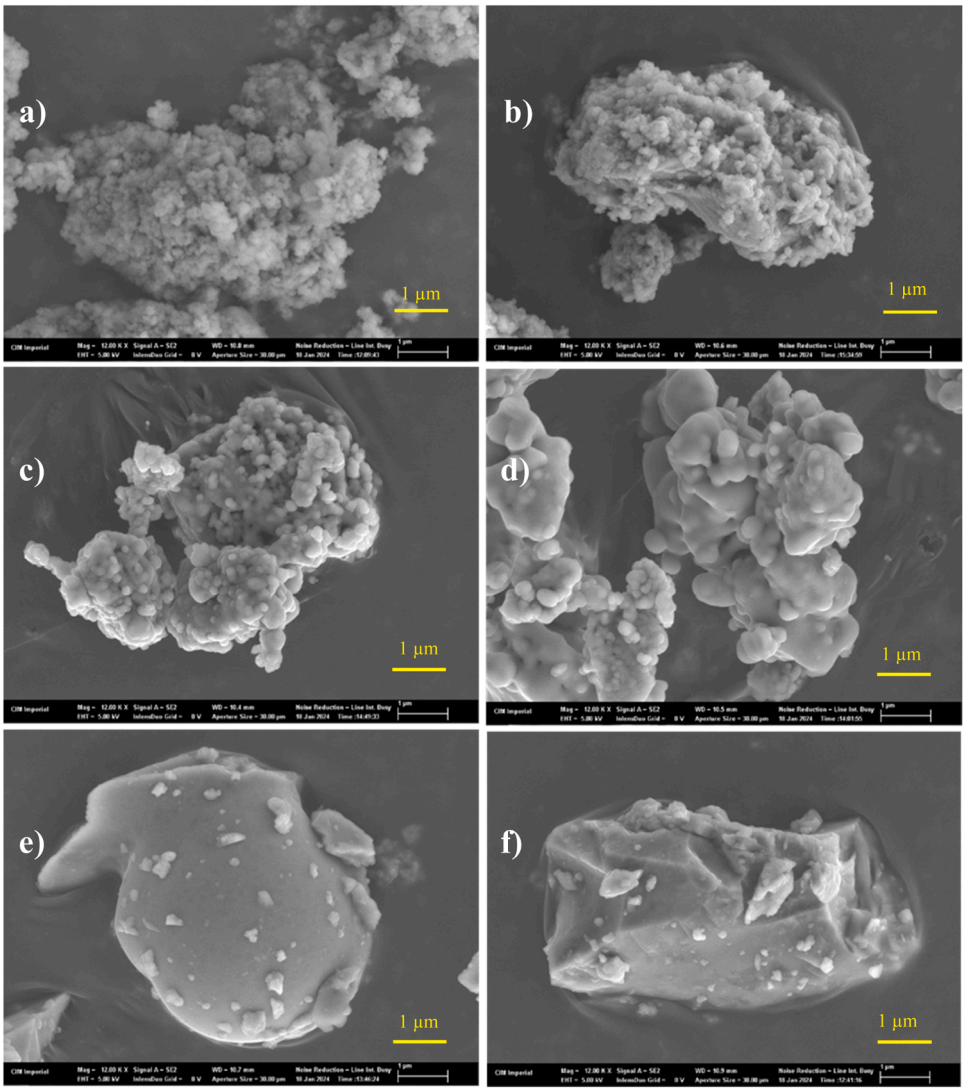

Fig. 4. SEM-SE images of raw and heat-treated silica-rich residue samples. a) SR untreated, b) SR840, c) SR870, d) SR900, e) SR950, f) SR1000.

Table 2
Particle size (d_{10}, d_{50} and d_{90}) values of raw and heat-treated silica-rich residue and commercial SCMs.

Sample	Particle size (µm)		
	d_{10}	d_{50}	d_{90}
SR untreated	6.7 ± 0.0	40.6 ± 0.3	130.6 ± 2.2
SR840	7.5 ± 0.0	61.6 ± 0.4	180.4 ± 1.6
SR870	8.9 ± 0.1	64.7 ± 1.4	180.0 ± 3.1
SR900	10.1 ± 0.2	65.6 ± 2.0	172.0 ± 3.0
SR950	14.5 ± 0.4	93.9 ± 1.5	230.6 ± 3.4
SR1000	21.7 ± 0.1	124.8 ± 0.8	297.2 ± 1.6
FA	3.2 ± 0.1	23.4 ± 0.2	99.0 ± 2.6
GGBFS	1.7 ± 0.0	10.1 ± 0.2	27.2 ± 0.6
SF	0.03 ± 0.0	0.14 ± 0.0	64.0 ± 0.3

and 900℃ generates highly pozzolanic materials, with specific surface area lower than directly carbonated waste concrete powder and comparable to commonly used SCMs [8,21].

3.2. Heat of hydration of paste samples

Fig. 6 shows the heat flow and cumulative heat of hydration from isothermal conduction calorimetry of cement pastes over 7 days. The main peak at ~8 h in Fig. 6a indicates C3S hydration, with a shoulder that relates to sulphate depletion and C3A reaction. According to literature, the aluminosilicate gel does not impact the hydration of silicates but accelerate the C3A hydration and sulfate depletion because of its high surface area and amorphous nature [12]. However, in this research the main peak for the paste containing untreated SR is delayed by ~24 hours. This is due to the retarding effect of the significantly large amount of superplasticiser, forming complexation with Ca^{2+} and inhibiting ion diffusion [42]. Compared to P-Ref, the shoulder corresponding to sulphate depletion occurs earlier for all blended pastes with heat-treated SR, because of the higher content of aluminosilicate gel. In Fig. 6b, all blended pastes with heat-treated SR show a higher C3S hydration peak and cumulative heat than the 100 % CEM I reference paste, indicating the pozzolanic reactivity and filler effect of SR. P-840, P-870 and P-900 have higher 7-day cumulative heat of hydration than P-950 and P-1000. Compared to common SCMs, these are lower than P-GGBFS but comparable to P-SF and higher than P-FA. This is consistent with the differences in pozzolanic reactivity of the heat-treated SR and common SCMs (Fig. 5a). It has been reported that the hydration heat at 72 h of cement paste containing 20 % of directly carbonated waste concrete powder is 322 J/g CEM I [21]. In comparison, the 72-h hydration heat of P-840, P-870 and P-900 are around 295 J/g CEM I. Given the lower water/cement content used in this research (0.4 versus 0.5 in the reported work), the pozzolanic reactivity of optimally heat-treated SR is

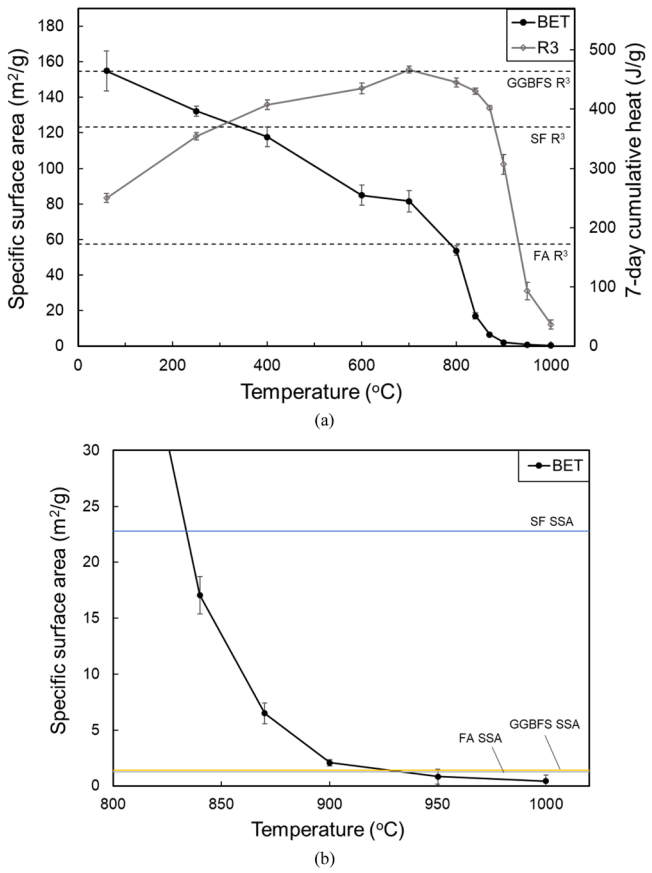

Fig. 5. (a) Variation in BET specific surface area and 7-day cumulative heat from R^3 test of the silica-rich residue against temperature. The 7-day R^3 heat of SF, FA and GGBFS are marked as horizontal dashed lines. (b) Comparison of the specific surface area of SR treated from 840°C to 1000°C and commonly used SCMs. The BET specific surface area of SF, FA and GGBFS are 22.80 ± 0.74, 1.26 ± 0.54 and 1.42 ± 0.30 m^2/g, respectively and marked as horizontal solid lines. Error bars show the standard deviation of the results.

comparable to that of carbonated waste concrete powder.

3.3. Flow and compressive strength of mortar

The flow table results are presented in Fig. 7. It is observed that the mortar containing untreated SR has the lowest workability of all the test mortars. This results in poorly compacted samples that have substantial surface voids even after extended vibration. In comparison, the flow of mortars containing heat-treated SR increased by 11.5 %, 16.2 %, 26.3 %, 37.0 % and 38.4 % for samples heated to 840, 870, 900, 950 and 1000°C compared to the untreated SR. Furthermore, mortars containing heat-treated SR show improved flow properties compared to silica fume. The improved workability helps samples to achieve good compaction without requiring superplasticizer.

Fig. 8 presents the compressive strength data of mortars containing untreated and heat-treated SR, compared to those containing 100 % CEM I (M-Ref) and 20 % CEM I replaced with FA, GGBFS or SF. The strength of mortars containing untreated SR is less than 10 MPa and increases marginally after 7 days, due to poor workability and inadequate compaction. Mortars with heat-treated SR up to 900°C show an increase in compressive strength at all ages with increasing temperature, due to improvements in workability and pozzolanic reactivity. Mortars with heat-treated SR (up to 900°C) have higher strengths than M-FA, and comparable strengths to M-Ref, M-GGBFS and M-SF. The later age strength gain is related to (i) the pozzolanic reaction of SR and (ii) the continuous consumption of $Ca(OH)_2$ by the C-(A)-S-H phase with low Ca/Si ratio formed from the pozzolanic reaction of SR at early ages to form C-(A)-S-H with high Ca/Si ratio [7]. Increasing heat treatment temperature above 900°C causes a reduction in pozzolanic reactivity and this outweighs the benefits of improved workability, as shown in the reduced 28-day and 60-day strength of M-950 and M-1000. This is due to the increased content of inert cristobalite, anorthite and hematite phases, as shown in the XRD data (Fig. 2).

In general, SR900 gives good workability, higher early-age strength and similar long-term strength compared to SR treated at other temperatures. Therefore, 900°C is considered the optimal temperature for improving the performance of aluminosilicate residue extracted from waste concrete powder.

3.4. Microstructure of mortars containing SR

Fig. 9a-f shows the SEM-BSE images of M-Ref, M-FA, M-SF, M-GGBFS, M-900 and M-1000. The microstructure of mortars consists of anhydrous clinker, hydration products, SCM particles and pores, which are clearly identified in the images. C-S-H phase and portlandite nucleates on the surface of the partially hydrated clinker particles and the SCMs. M-900 forms dense microstructure similar to M-SF and M-GGBFS and less porous than M-FA. In M-FA and M-900, needle-shaped AFm crystals can be observed on the rim of the SCM grains (Fig. S1). SR900 generates more needle-shaped crystals than FA. This is due to its stronger pozzolanic reactivity generated from the amorphous aluminosilicate gel.

The composition of C-S-H phase of M-900 is compared to M-Ref, M-1000 which represents the mortar with inert filler and M-GGBFS which represents the mortar with a highly reactive SCM in Fig. 10 using SEM-EDS analysis. The EDS sampling points are marked in Fig. S2. The Si/Ca ratio of C-S-H phase increases from 0.49 ± 0.07 in M-GGBFS, 0.53 ± 0.06 in M-1000 and 0.54 ± 0.06 in M-Ref to 0.58 ± 0.07 in M-900. The Al/Ca ratio increased from 0.06 ± 0.02 in M-Ref to 0.09 ± 0.03 in M-1000 and M-GGBFS and further to 0.10 ± 0.03 in M-900, respectively. This is due to the pozzolanic reaction of the amorphous aluminosilicate gel in the composite cement which gives higher Si/Ca and Al/Ca ratios compared to neat CEM I and composite cements with inert filler and slag [43].

4. Discussion

This research has shown that heat treatment can reduce the surface area of the aluminosilicate residue extracted from cement paste. Optimum heat treatment at 900°C preserves the glassy aluminosilicate structure and maintains high pozzolanic reactivity. This is a lower temperature than what is used in traditional sintering processes, which are typically above 1000°C, because the aluminosilicate residue contains small amounts of CaO and MgO which act as a flux to lower the sintering temperature [44]. This temperature is also much lower than the temperature required to make cement clinker (1450°C) and could be achieved using biomass or other green, low carbon energy such as residual heat [45].

At the optimal temperature, the specific surface area of SR was reduced by 99 % compared to untreated SR, and the specific surface area was 2.09 m^2/g, which is just slightly higher than that for blast furnace slag and fly ash. Furthermore, the cumulative heat release of SR900 after 7 days in the R^3 test was increased by 22.8 % compared to the untreated SR, while the loss in pozzolanic reactivity compared to SR700 (34.3 %) is acceptable. In comparison to the directly carbonated waste concrete powder, SR900 has 96.3 % lower surface area and improves the workability by 40 % at 20 % clinker replacement [21]. Direct comparison of the mechanical performance of heat-treated SR and directly carbonated waste concrete powder is difficult because of the different particle size of fine aggregate and mixing ratio used in preparing mortar samples. Alternatively, comparisons can be made by examining the compressive strength gain versus the inert reference. The 20-mm cube mortar

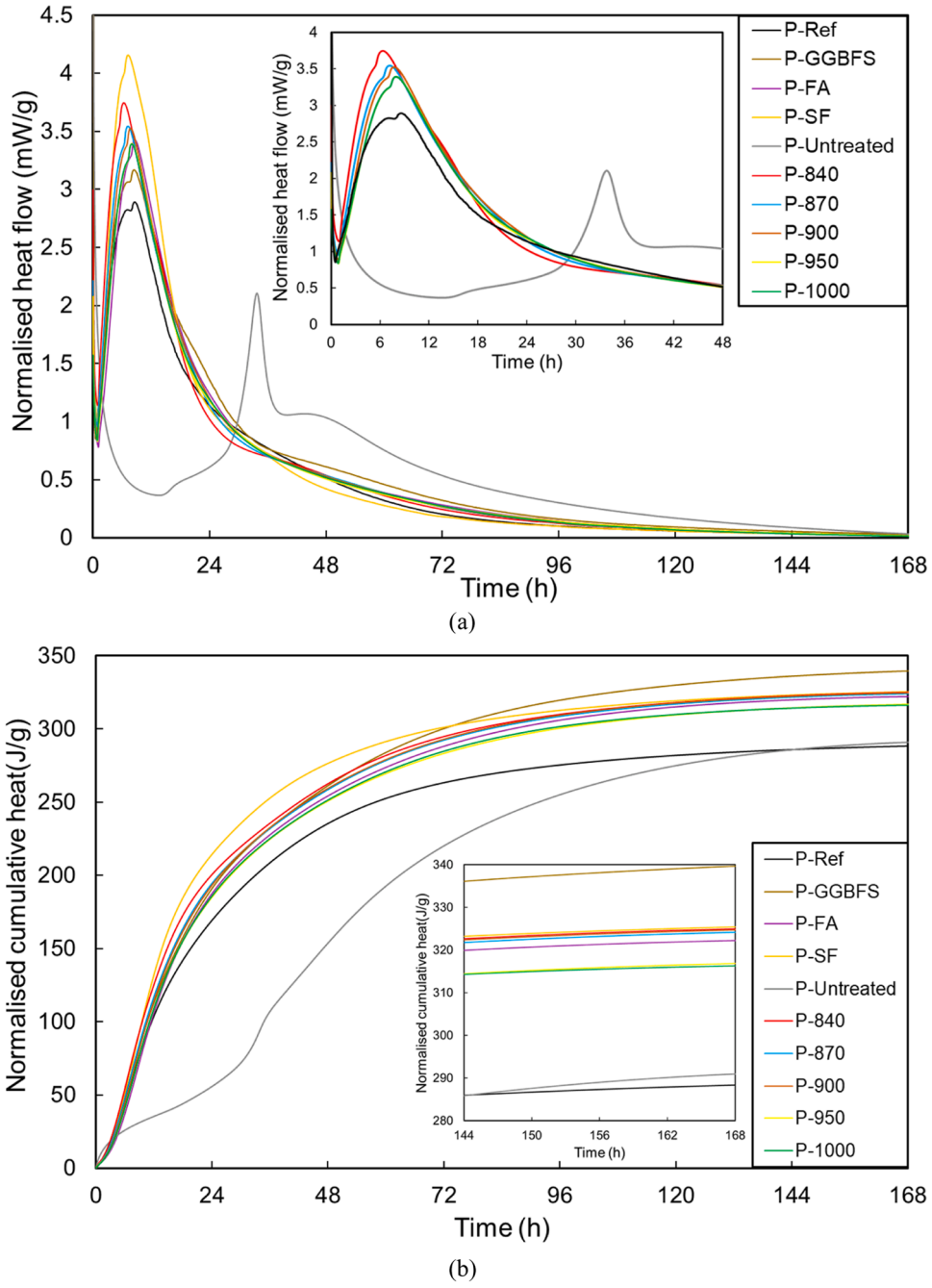

Fig. 6. Isothermal conduction calorimetry curves showing (a) heat flow and (b) cumulative heat of hydration of cement pastes (P-) containing 100 % CEM I (P-Ref) and 20 % replacement with SRs and other SCMs (GGBFS, FA, SF).

samples, using 20 % of CEM I replaced by directly carbonated waste concrete powder, and sand less than 0.4 μm, mixed at a sand: binder: water ratio of 1:1:0.55 have a ~16 % higher 28-day compressive strength (50 MPa) than reference with limestone filler (43 MPa) [7]. The 28-day compressive strength of M-900 (43.5 MPa) is 34 % higher than that of M-1000 (32.4 MPa), which is regarded as an inert reference. The results show that heat treatment of SR extracted from cement paste can improve the workability and strength of mortars, making it a viable candidate as an alternative SCM. Also, the indirect carbonation process can produce purer $CaCO_3$ for use in other value-added applications.

Crystallization of SR occurs above 900℃, as it transforms into cristobalite, anorthite and hematite. The crystallization process redistributes network modifier ions (Al^{3+}, Fe^{3+} and Ca^{2+}), and this reduces pozzolanic reactivity. Non-reactive crystalline phases reduce the surface area [40]. Additionally, the degree of polymerization of the remaining reactive amorphous aluminosilicate is increased due to the loss of network modifier ions, resulting in a reduction in pozzolanic reactivity [46]. It is therefore important to keep the heat treatment temperature below 950℃ to avoid these effects.

Construction and demolition waste and particularly end-of-life concrete needs to be properly valorised. Crushed concrete fines are a problematic waste but this work shows that this should be regarded as a valuable resource. Extracting SR using indirect carbonation of crushed concrete fines can form new SCMs, and this is an essential step towards achieving circular concrete. Based on this research, it was found that 1 kg of hydrated cement powder produces ~0.2 kg of heat-treated SR. Waste concrete powder constitutes ~30 % of the total waste concrete [5]. Based on the current global production of waste concrete of ~2

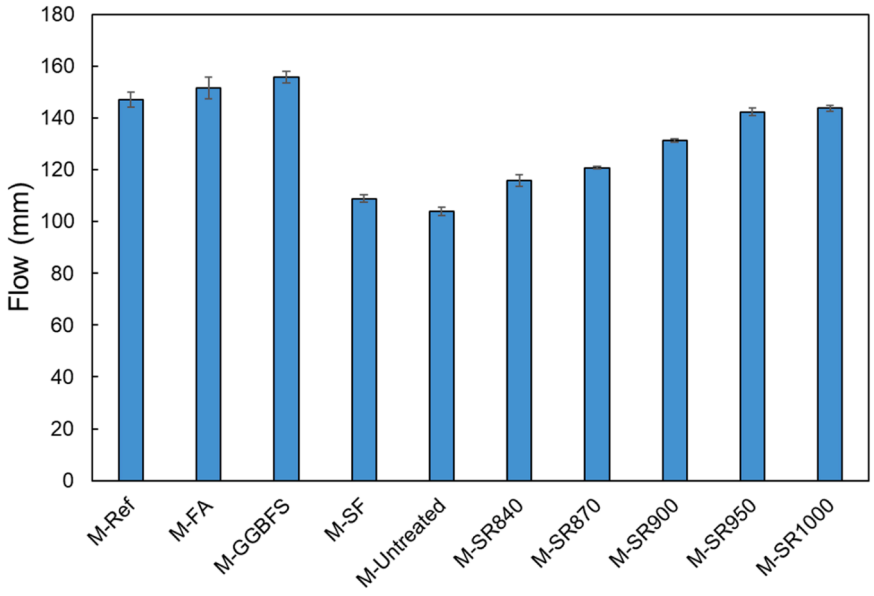

Fig. 7. Flow values of the test mortars at 0.56 w/b ratio. M-ref contains 100 % CEM I 52.5 N. Other mortar samples contain 20 % CEM I replaced with SR or conventional SCM. Error bars show the standard deviation of the results.

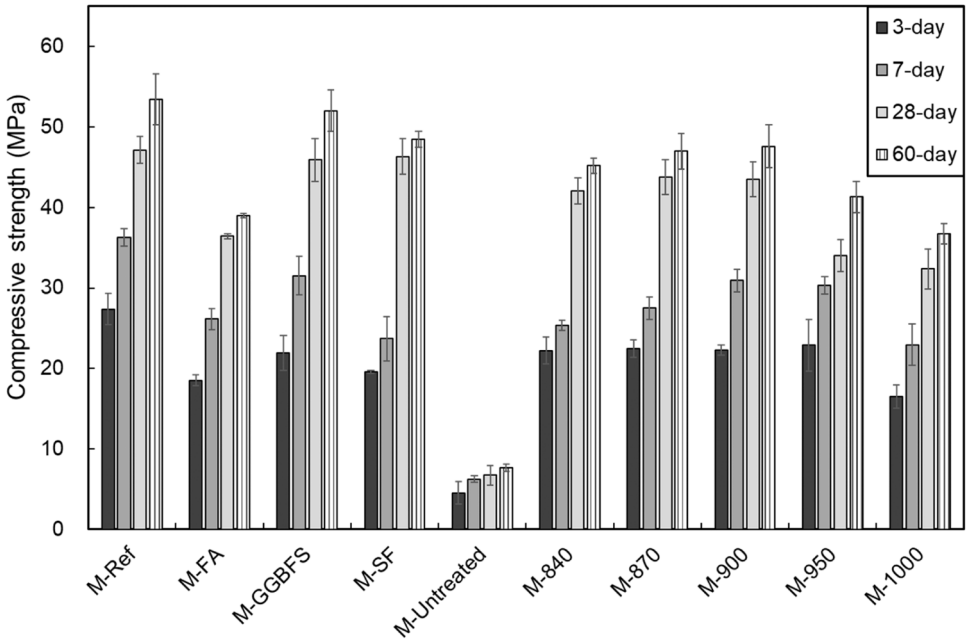

Fig. 8. Compressive strength of test mortars at 3, 7, 28 and 60 days. Error bars show the standard deviation of the results.

billion tonnes per annum, 120 million tonnes of heat-treated SR could be produced, and this is expected to increase as ageing concrete infrastructure reaches end-of-life and is demolished. Therefore, aluminosilicates from waste concrete can be an important supplement to existing SCMs and contribute to higher clinker replacement levels. Further research will focus on the performance of heat-treated SR at higher clinker replacement ratios and the detailed evaluation of energy consumption and embedded carbon emissions of this material.

5. Conclusions

The viability of the aluminosilicate residue produced by acid leaching of cement paste to form supplementary cementitious materials can be improved by thermal treatment. The optimum heat treatment temperature is ~900℃. At this temperature, the heat-treated aluminosilicate residue has a comparable specific surface area and pozzolanic reactivity to commercially available SCMs. Higher temperatures result in crystallisation of cristobalite, anorthite and hematite, reducing pozzolanic reactivity, while lower temperatures result in insufficient reduction in surface area. Mortars with 20 % cement replacement of optimally heat-treated aluminosilicate residue have good workability and higher compressive strengths than mortars containing fly ash, and this is comparable to mortars containing SF and GGBFS. The results indicate that acid treatment of waste concrete combined with indirect carbonation of the leachate and thermal treatment of the aluminosilicate residue, when combined with associated recovery of clean sand and aggregate, represents a potential way to achieve low-carbon circular concrete.

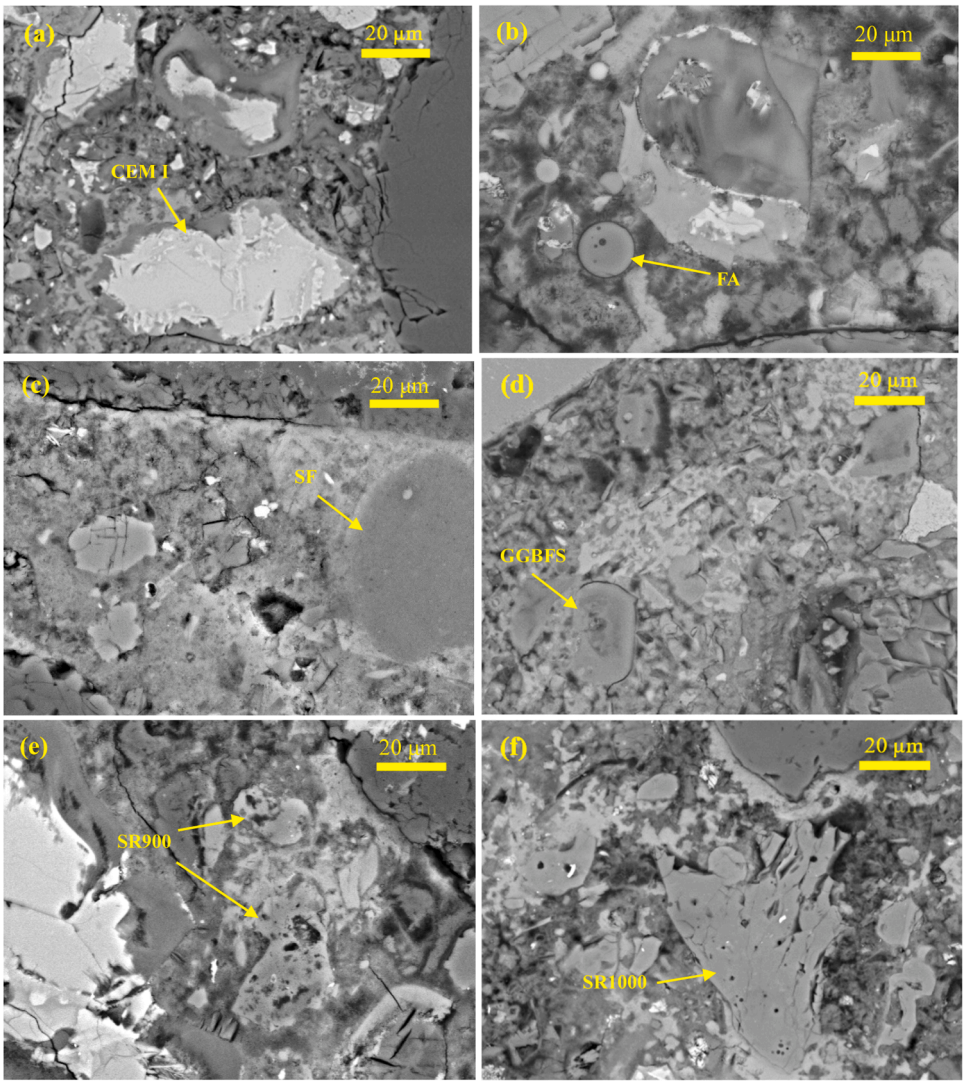

Fig. 9. SEM-BSE images of 28-day mortars. (a) M-Ref; (b) M-FA; (c) M-SF; (d) M-GGBFS; (e) M-900; (f) M-1000.

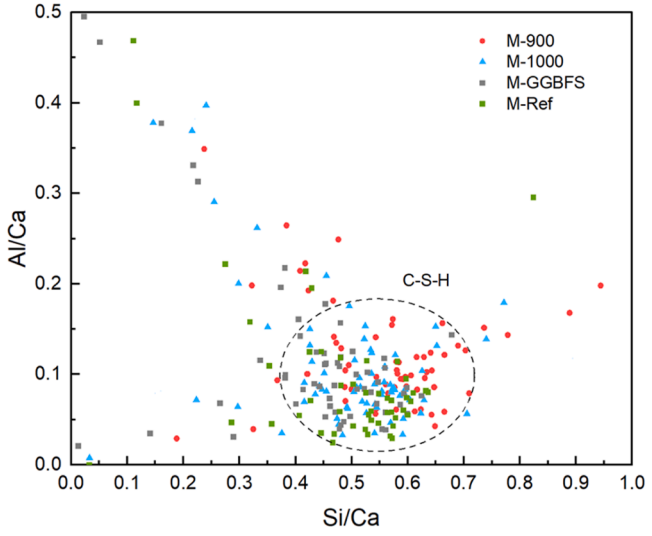

Fig. 10. 2D scatter plot of EDS analysis of C-S-H composition on 28-day mortar samples. The sampling points related to C-S-H are marked with a dashed ellipse.

CRediT authorship contribution statement

Christopher Cheeseman: Writing – review & editing, Supervision, Conceptualization. **Hong Wong:** Writing – review & editing, Supervision, Conceptualization. **Marcus Yio:** Writing – review & editing, Resources, Methodology. **Suyang Zhang:** Writing – review & editing, Visualization, Methodology, Conceptualization. **Tiejun Ding:** Writing – review & editing, Writing – original draft, Visualization, Validation, Methodology, Conceptualization.

Declaration of Competing Interest

The authors declare that they have no known competing financial interests or personal relationships that could have appeared to influence the work reported in this paper.

Acknowledgement

The research leading to this publication benefitted from EPSRC funding under grant No. EP/R010161/1 and from support from the UKCRIC Coordination Node, EPSRC grant number EP/R017727/1, which funds UKCRIC's ongoing coordination. We acknowledge the assistance from Andrew Morris and Les Clark in the laboratory work.

Appendix A. Supporting information

Supplementary data associated with this article can be found in the online version at doi:10.1016/j.conbuildmat.2025.139981.

Data availability

Data will be made available on request.

References

[1] R. Islam, T.H. Nazifa, A. Yuniarto, A.S.M. Shanawaz Uddin, S. Salmiati, S. Shahid, An empirical study of construction and demolition waste generation and implication of recycling, Waste Manag. 95 (2019) 10–21, https://doi.org/10.1016/j.wasman.2019.05.049.

[2] P. Villoria Sáez, M. Osmani, A diagnosis of construction and demolition waste generation and recovery practice in the European Union, J. Clean. Prod. 241 (2019), https://doi.org/10.1016/j.jclepro.2019.118400.

[3] L. Evangelista, M. Guedes, J. De Brito, A.C. Ferro, M.F. Pereira, Physical, chemical and mineralogical properties of fine recycled aggregates made from concrete waste, Constr. Build. Mater. 86 (2015) 178–188, https://doi.org/10.1016/j.conbuildmat.2015.03.112.

[4] J. Xiao, W. Li, Z. Sun, D.A. Lange, S.P. Shah, Properties of interfacial transition zones in recycled aggregate concrete tested by nanoindentation, Cem. Concr. Compos 37 (2013) 276–292, https://doi.org/10.1016/j.cemconcomp.2013.01.006.

[5] C.S. Poon, P. Shen, Y. Jiang, Z. Ma, D. Xuan, Total recycling of concrete waste using accelerated carbonation: A review, Cem. Concr. Res 173 (2023), https://doi.org/10.1016/j.cemconres.2023.107284.

[6] J. Wang, M. Mu, Y. Liu, Recycled cement, Constr. Build. Mater. 190 (2018) 1124–1132, https://doi.org/10.1016/j.conbuildmat.2018.09.181.

[7] M. Zajac, J. Song, J. Skocek, M. Ben Haha, J. Skibsted, Composite cements with aqueous and semi-dry carbonated recycled concrete pastes, Constr. Build. Mater. 407 (2023), https://doi.org/10.1016/j.conbuildmat.2023.133362.

[8] M. Zajac, J. Skocek, J. Gołek, Deja, Supplementary cementitious materials based on recycled concrete paste, J. Clean. Prod. 387 (2023), https://doi.org/10.1016/j.jclepro.2022.135743.

[9] H.J. Ho, A. Iizuka, E. Shibata, H. Tomita, K. Takano, T. Endo, CO2 utilization via direct aqueous carbonation of synthesized concrete fines under atmospheric pressure, ACS Omega (2020), https://doi.org/10.1021/acsomega.0c00985.

[10] P. Shen, Y. Jiang, Y. Zhang, S. Liu, D. Xuan, J. Lu, S. Zhang, C.S. Poon, Production of aragonite whiskers by carbonation of fine recycled concrete wastes: An alternative pathway for efficient CO2 sequestration, Renew. Sustain. Energy Rev. 173 (2023), https://doi.org/10.1016/j.rser.2022.113079.

[11] P. Shen, Z. Gu, J. Lu, Y. Zhang, Y. Jiang, D. Xuan, S. Zhang, C.S. Poon, Preparation of reactive urchin-like recycled concrete aggregate by wet carbonation: Towards improving the bonding capability of the interfacial transition zone in recycled aggregate concrete, Cem. Concr. Compos 143 (2023), https://doi.org/10.1016/j.cemconcomp.2023.105235.

[12] M. Zajac, J. Skocek, P. Durdzinski, F. Bullerjahn, J. Skibsted, M. Ben, R. Global, D. H. Ag, Effect of carbonated cement paste on composite cement hydration and performance, Cem. Concr. Res 134 (2020) 106090, https://doi.org/10.1016/j.cemconres.2020.106090.

[13] G. Pan, M. Zhan, M. Fu, Y. Wang, X. Lu, Effect of CO2 curing on demolition recycled fine aggregates enhanced by calcium hydroxide pre-soaking, Constr. Build. Mater. 154 (2017) 810–818, https://doi.org/10.1016/j.conbuildmat.2017.07.079.

[14] H. Mehdizadeh, K.H. Mo, T.C. Ling, CO2-fixing and recovery of high-purity vaterite CaCO3 from recycled concrete fines, Resour. Conserv Recycl 188 (2023), https://doi.org/10.1016/j.resconrec.2022.106695.

[15] P. Chen, J. Wang, L. Wang, Y. Xu, X. Qian, H. Ma, Producing vaterite by CO2 sequestration in the waste solution of chemical treatment of recycled concrete aggregates, J. Clean. Prod. 149 (2017) 735–742, https://doi.org/10.1016/j.jclepro.2017.02.148.

[16] X. Fang, D. Xuan, B. Zhan, W. Li, C.S. Poon, A novel upcycling technique of recycled cement paste powder by a two-step carbonation process, J. Clean. Prod. 290 (2021) 125192, https://doi.org/10.1016/j.jclepro.2020.125192.

[17] X. Fang, D. Xuan, B. Zhan, W. Li, C.S. Poon, Characterization and optimization of a two-step carbonation process for valorization of recycled cement paste fine powder, Constr. Build. Mater. 278 (2021) 122343, https://doi.org/10.1016/j.conbuildmat.2021.122343.

[18] T. Ding, H. Wong, X. Qiao, C. Cheeseman, Developing circular concrete: Acid treatment of waste concrete fines, J. Clean. Prod. 365 (2022) 132615, https://doi.org/10.1016/j.jclepro.2022.132615.

[19] K. Scrivener, F. Martirena, S. Bishnoi, S. Maity, Calcined clay limestone cements (LC3), Cem. Concr. Res 114 (2018) 49–56, https://doi.org/10.1016/j.cemconres.2017.08.017.

[20] R. Supriya, U. Chaudhury, P.C. Sharma, L.P. Thapliyal, Singh, Low-CO2 emission strategies to achieve net zero target in cement sector, J. Clean. Prod. 417 (2023), https://doi.org/10.1016/j.jclepro.2023.137466.

[21] L. Peng, Y. Jiang, J. Ban, Y. Shen, Z. Ma, Y. Zhao, P. Shen, C.S. Poon, Mechanism underlying early hydration kinetics of carbonated recycled concrete fines-ordinary portland cement (CRCF-OPC) paste, Cem. Concr. Compos 144 (2023), https://doi.org/10.1016/j.cemconcomp.2023.105275.

[22] Y. Mao, S. Drissi, X. Hu, J. Zhang, C. Shi, Effect of wet carbonated recycled cement paste powder on the rheology of cement paste, Cem. Concr. Res 181 (2024) 107553, https://doi.org/10.1016/j.cemconres.2024.107553.

[23] T. Ding, H. Wong, M. Yio, C. Cheeseman, Production of amorphous aluminosilicate and vaterite from acid leaching of hydrated cement paste, J. Sustain Cem. Based Mater. (2024) 1–12, https://doi.org/10.1080/21650373.2024.2397484.

[24] Z. Song, X. Zhang, Y. Tan, Q. Zeng, Y. Hua, X. Wu, M. Li, X. Liu, M. Luo, An all-in-one strategy for municipal solid waste incineration fly ash full resource utilization by heat treatment with added kaolin, J. Environ. Manag. 329 (2023), https://doi.org/10.1016/j.jenvman.2022.117074.

[25] M. Ilic, C. Cheeseman, C. Sollars, J. Knight, Mineralogy and microstructure of sintered lignite coal fly ash, Fuel 82 (2003) 331–336. ⟨www.fuelfirst.com⟩.

[26] J.J. Biernacki, A.K. Vazrala, H. Wayne Leimer, Sintering of a class F fly ash, Fuel 87 (2008) 782–792, https://doi.org/10.1016/j.fuel.2007.08.024.

[27] ASTM C1897-20, Standard Test Methods for Measuring the Reactivity of Supplementary Cementitious Materials by Isothermal Calorimetry and Bound Water Measurements, (2020).

[28] BS EN 196-11:2018, Methods of testing cement. Part 11: Heat of Hydration - Isothermal Conduction Calorimetry method, 2018.

[29] L.T. Zhuravlev, The surface chemistry of amorphous silica. Zhuravlev model, Colloids Surf. A Physicochem Eng. Asp. 173 (2000) 1–38. ⟨www.elsevier.nl/locate/colsurfa⟩.

[30] C.J. Brinker, S.P. Mukherjee, Conversion of monolithic gels to glasses in a multicomponent silicate glass system, J. Mater. Sci. 16 (1981) 1980–1988.

[31] A. Pramanik, K. Bhattacharjee, M.K. Mitra, G.C. Das, B. Duari, A mechanistic study of the initial stage of the sintering of sol-gel derived silica nanoparticles, Int. J. Mod. Eng. Res. 3 (2013) 1066–1070.

[32] T. Hirono, S. Kaneki, T. Ishikawa, J. Kameda, N. Tonoike, A. Ito, Y. Miyazaki, Generation of sintered fault rock and its implications for earthquake energetics and fault healing, Commun. Earth Environ. 1 (2020), https://doi.org/10.1038/s43247-020-0004-z.

[33] P.E. Imoisili, T.-C. Jen, Synthesis and characterization of amorphous nano silica from South African coal fly ash, Mater. Today Proc. (2023), https://doi.org/10.1016/j.matpr.2023.06.077.

[34] M. Mohammadi, M. Khanmohammadi Khorrami, H. Vatanparast, H. Ghasemzadeh, Prediction of surface tension of solution in the presence of hydrophilic silica nanoparticle and anionic surfactant by ATR-FTIR spectroscopy and chemometric methods, Spectrochim. Acta A Mol. Biomol. Spectrosc. 255 (2021), https://doi.org/10.1016/j.saa.2021.119697.

[35] P.E. Imoisili, K.O. Ukoba, T.C. Jen, Green technology extraction and characterisation of silica nanoparticles from palm kernel shell ash via sol-gel, J. Mater. Res. Technol. 9 (2020) 307–313, https://doi.org/10.1016/j.jmrt.2019.10.059.

[36] E.A. Paukshtis, M.A. Yaranova, I.S. Batueva, B.S. Bal'zhinimaev, A FTIR study of silanol nests over mesoporous silicate materials, Microporous Mesoporous Mater. 288 (2019), https://doi.org/10.1016/j.micromeso.2019.109582.

[37] S. Zhang, S. Tie, F. Zhang, Cristobalite formation from the thermal treatment of amorphous silica fume recovered from the metallurgical silicon industry, Micro Nano Lett. 13 (2018) 1465–1468, https://doi.org/10.1049/mnl.2018.5167.

[38] G. Yilmaz, Structural characterization of glass-ceramics made from fly ash containing SiO2-Al2O3-Fe2O3-CaO and analysis by FT-IR-XRD-SEM methods, J. Mol. Struct. 1019 (2012) 37–42, https://doi.org/10.1016/j.molstruc.2012.03.028.

[39] F. Silencieux, M. Bouchoucha, O. Mercier, S. Turgeon, P. Chevallier, F. Kleitz, M. A. Fortin, Mesoporous silica nanoparticles under sintering conditions: a quantitative study, Langmuir 31 (2015) 13011–13021, https://doi.org/10.1021/acs.langmuir.5b02961.

[40] P. de Azevedo Basto, V. Estolano de Lima, A. de Melo Neto, Capability of R3 test to evaluate pozzolanicity of ground raw and calcined sugarcane bagasse ashes, Mater. Today Proc. (2023), https://doi.org/10.1016/j.matpr.2023.04.048.

[41] R.D. Kalina, S. Al-Shmaisani, R.D. Ferron, M.C.G. Juenger, False positives in ASTM C618 specifications for natural pozzolans, Acids Mater. J. 116 (2019).

[42] F. Puertas, H. Santos, M. Palacios, S. Martínez-Ramírez, Polycarboxylate superplasticiser admixtures: effect on hydration, microstructure and rheological behaviour in cement pastes, Adv. Cem. Res. 17 (2005) 77–89, https://doi.org/10.1680/adcr.2005.17.2.77.

[43] B. Lothenbach, K. Scrivener, R.D. Hooton, Supplementary cementitious materials, Cem. Concr. Res. 41 (2011) 1244–1256, https://doi.org/10.1016/j.cemconres.2010.12.001.

[44] Y. Huang, Z. Bian, W. Ji, M. Yio, Z. Chen, J.X. Lu, C. Cheeseman, C.S. Poon, Production of glass-ceramic aggregates from solid wastes for high-strength and low-shrinkage lightweight mortars, Constr. Build. Mater. 416 (2024), https://doi.org/10.1016/j.conbuildmat.2024.135244.

[45] M. Li, F. Zheng, Y. Xiao, Y. Guan, J. Wang, Q. Zhen, Y. Yu, Utilization of residual heat to prepare high performance foamed glass-ceramic from blast furnace slag and its reinforce mechanism, Process Saf. Environ. Prot. 156 (2021) 391–404, https://doi.org/10.1016/j.psep.2021.10.019.

[46] J. Skibsted, R. Snellings, Reactivity of supplementary cementitious materials (SCMs) in cement blends, Cem. Concr. Res. 124 (2019), https://doi.org/10.1016/j.cemconres.2019.105799.